M1 Polarization bias and subsequent NASH progression is attenuated by nitric oxide donor DETA NONOate via inhibition of CYP2E1 induced oxidative stress in obese mice

Ratanesh Kumar Seth, Suvarthi Das, Sahar Pourhoseini, Diptadip Dattaroy, Stephen Igwe, Julie Basu Ray, Daping Fan, Gregory A. Michelotti, Anna Mae Diehl and Saurabh Chatterjee

1. Environmental Health and Disease Laboratory, Department of Environmental Health Sciences, Arnold School of Public Health, University of South Carolina, Columbia SC 29208 (R.K.S.,S.D., S.P., D.D.,S.C.). School of Science, Technology, Engineering and Mathematics (STEM), Dillard University, New Orleans, LA 70122. (S.I., J.B.R.), Department of Cell Biology and Anatomy, University of South Carolina School of Medicine, Columbia SC 29209 (D.P., M.N.), Division of Gastroenterology, Duke University, Durham NC 27707. (G.A.M., A.M.)

Running title: NO donor attenuates inflammation in NASH liver

List of non-standard abbreviations: DETA NONOate: Z)-1-[N-(2-aminoethyl)-N-(2-ammonioethyl)amino]diazen-1-ium-1,2-diolate

Author for correspondence:

*Dr. Saurabh Chatterjee, Ph.D. [1]Environmental Health and Disease Laboratory, Department of Environmental Health Sciences, University of South Carolina, Columbia 29208 USA. Email: schatt@mailbox.sc.edu; Tel: 803-777-8120; Fax: 803-777-3391

Conflict of interest: The authors declare no conflict of interest.

Abstract: 239 words.

Introduction: 749 words

Discussion: 1362 words

Figures: 7

Manuscript+references: 35 pages

Abstract:

Activation of M1 macrophages in the nonalcoholic steatohepatitis (NASH) following several external or endogenous factors viz inflammatory stimuli, oxidative stress and cytokines are known. However, any direct role of oxidative stress in causing M1 polarization in NASH has been unclear. We hypothesized that CYP2E1-mediated oxidative stress causes M1 polarization in experimental NASH and NO donor administration inhibits CYP2E1 mediated inflammation with concomitant attenuation of M1 polarization. Since CYP2E1 takes center stage in these studies we use a toxin model of NASH which uses a ligand and a substrate of CYP2E1 for inducing NASH. Subsequently we use a methionine and choline deficient diet induced rodent NASH model where CYP2E1 role in disease progression has been shown. Results show that CYP2E1 causes M1 polarization bias that includes a significant increase in IL-1β and IL-12 in both models of NASH while CYP2E1 null mice or diallyl sulfide administration prevented it. Administration of $GdCl_3$, a macrophage toxin attenuated both the initial M1 response and subsequent M2 response showing the observed increase in cytokine levels is primarily from macrophages. Based on the evidence of an adaptive NO increase, NO donor administration in vivo, that mechanistically inhibited CYP2E1 catalyzed oxidative stress during the entire study in NASH abrogated M1 polarization and NASH progression. The results obtained show the association of CYP2E1 in M1 polarization and that inhibition of CYP2E1 catalyzed oxidative stress by NO donor (DETA NONOate) can be a promising therapeutic strategy in NASH.

Introduction:

Nonalcoholic steatohepatitis (NASH) can be characterized by inflammation, hepatocyte necrosis, and often fibrosis (Bohinc and Diehl, 2012). If unchecked, NASH can rapidly progress to cirrhosis and hepatocellular carcinoma.

To make matters worse, NASH treatment is further complicated by the absence of a proven treatment regimen due to the silent nature of the disease and patients reporting to clinics at an advanced stage (Cheung and Sanyal, 2009). The two hit or multi hit paradigms can range from defective triglyceride production and release, free fatty acid content, oxidative stress, damage associated molecular patterns, cytokine release and more recently xenobiotic enzymes like the cytochrome p450s (Tilg and Moschen, 2008; Tilg and Moschen, 2010; Abdelmegeed et al., 2012; Abdelmegeed et al., 2013). A recent report in NASH rodent model, coupled with several research reports in alcoholic steatohepatitis clearly ascribe the role of CYP2E1 in generation of oxygen species that can act as a second hit for progression of NASH (Caro and Cederbaum, 2004; Aubert et al., 2011; Abdelmegeed et al., 2013). The second hit can couple the proinflammatory changes to the liver microenvironment and aid in the progression of severe end stage NASH complications that may include fibrosis and hepatocellular carcinoma.

Inflammation is central to NASH progression (Tilg and Moschen, 2008; Bohinc and Diehl, 2012; Ganz and Szabo, 2013). We have shown previously that oxidant stress linked inflammation is closely associated with NASH progression (Chatterjee et al., 2012; Das et al., 2013b; Seth et al., 2014). Hepatocyte necrosis, lipid peroxidation and activation of purinergic receptor X7 (P2X7r) can give rise to NADPH oxidase activation

leading to Kupffer cell activation, a key event in NASH progression (Chatterjee et al., 2012; Das et al., 2013a). Also, proinflammatory cytokine induction was dependent on oxidative stress and CYP2E1 in a toxin model of NASH (Das et al., 2013a). In a recent report, Sutti S et al showed that when mice were immunized with malonyldialdehyde (MDA) adducted bovine serum albumin it did not affect control mice livers, but further stimulated transaminase release, lobular inflammation, and the hepatic expression of proinflammatory cytokine in methionine and choline deficient (MCD) diet fed mice which exhibits NASH (Sutti et al., 2014). The increased severity of NASH in immunized MCD-diet fed mice involved liver recruitment of the T helper (Th1 activation of CD41 T cells that, in turn, further stimulated macrophage M1 responses (Sutti et al., 2014). Though the rodent models of NASH have established the prominent role of CYP2E1 and its associated oxidative stress as key to NASH progression, the mechanisms of how CYP2E1 regulates inflammation, especially the polarization of macrophages and generation of a proinflammatory response has been unclear.

Recent published reports indicate a strong M1 bias following the inflammatory trigger (Maina et al., 2012). The M1 polarization is associated with higher nitric oxide, IL-1β, TNF-α, IFN-γ, IL-12 and several chemo attractants (Maina et al., 2012). This happens mostly in the initial phases of liver injury in rodent models which has been used to study NASH progression. Patients with early phases of NASH occurrences also have reciprocated a M1 bias (Bertola et al., 2010). However NASH progression is also associated with a delayed shift into profibrotic mechanisms which might require an M2 polarization. Inflammatory surges in many diseases are accompanied by a late M2 shift which can arise from a higher proinflammatory cytokine levels, higher nitric oxide (NO)

levels or both (Liu et al., 2014). High nitric oxide levels have been accompanied by higher arginase activity leading to release of TGF-β, IL-4 and IL-13 release, which are primarily anti-inflammatory but do contribute to the fibrotic process (Chatterjee et al., 2006; Liu et al., 2014). The role of higher nitric oxide levels in causing a feedback loop triggering anti-inflammatory mechanisms can be a potential therapeutic approach in NASH, given the use of nitric oxide donor (NO donor) in a single study for NASH remediation involving ob/ob (spontaneous knockout of leptin) mice where no mechanistic inputs were provided (de Oliveira et al., 2008). Coupled with boosting NO levels, the extensive studies that exist about the role of nitric oxide in inhibiting CYP2E1, the use of NO donor to treat NASH can be an excellent treatment regimen in NASH (Gergel et al., 1997; Aitken et al., 2008).

Based on the existing literature inputs we hypothesized that CYP2E1-mediated oxidative stress causes M1 polarization in experimental NASH and NO donor administration inhibits CYP2E1 mediated oxidative stress and inflammation with concomitant attenuation of M1 polarization. Since CYP2E1 takes center stage in these studies we use a toxin model of NASH which uses a ligand and a substrate of CYP2E1 for inducing NASH and subsequently we use a MCD diet induced rodent NASH model where CYP2E1 role in its progression has been shown. Results show that CYP2E1 causes M1 polarization bias in both models of NASH while CYP2E1 null mice prevents it. NO donor administration inhibits CYP2E1 mRNA, and CYP2E1-induced oxidative stress, M1 polarization and NASH progression.

Materials and Methods:

Materials

Bromodichloromethane (BDCM), gadolinium chloride ($GdCl_3$) and corn oil were purchased from Sigma Chemical Company, St Louis, MO. DETA NONOate (NO) was purchased from Cayman Chemical, MI. Diallyl sulfide (DAS) was purchased from Santa Cruz Biotechnology, Inc. Santa Cruz, CA. anti-4-hydroxynonenal (4-HNE), anti-IL-1β, anti-IL-13, anti-CYP2E1 and anti-α-smooth muscle actin (α-SMA) primary antibodies and secondary antibodies conjugated with HRP were purchased from AbCam Inc. (Cambridge, MA). anti-IL-12 antibody was purchased from Pierce Biotechnology, Rockford, IL. Secondary antibodies conjugated with fluorophore (Alexafluor 633) were purchased from Life technologies, Carlsbad, CA. Nitric Oxide Fluorometric Assay Kit was purchased from BioVision Incorporated, Milpitas, CA. 1400 W, the NOS2 inhibitor was purchased from Cayman Chemicals, CA. HNE-His Adduct ELISA Kit was purchased from Cell Biolabs, Inc., San Diego, CA. All experimental wild type and gene specific knockout mice were purchased from Jackson Laboratories, Bar Harbor, ME. Animal diets were purchased from Research Diets, Inc. New Brunswick, NJ. All other chemicals were of analytical grade and were purchased from Sigma Chemical Company unless otherwise specified.

Mouse model for toxin induced NASH

Pathogen-free, male, C57BL/6J background mice were used as wild type mice for diet induced obese model (DIO). Mice that contained the deleted CYP2E1 gene (29/Sv-*Cyp2e1*^{tm1Gonz}/J) (CYP2E1KO) and that contained the deleted NOS2 gene (B6.129P2-

JPET Fast Forward. Published on October 27, 2014 as DOI: 10.1124/jpet.114.218131
This article has not been copyedited and formatted. The final version may differ from this version.

Nos2^{tm1Lau}/J) (NOS2KO) were fed with a high fat diet and treated identically to DIO mice. The mice were housed one in each cage before any experimental use and fed with a high fat diet (60% kcal) from 6 weeks to 16 weeks.

Administration of bromodichloromethane (BDCM)-induction of liver injury

DIO mice and high-fat-diet fed gene specific knockout mice at 16 weeks were administered with BDCM (1.0 mmole/kg, diluted in corn oil) through the intra-peritoneal route, twice in a week, for one week to assess early stage of liver injury (DIO+BDCM (1w)) and for 4 weeks to assess the effects of chronic exposure of BDCM (DIO+BDCM (4w)). However, DIO mice and high-fat-fed gene-specific knockout mice treated with corn oil (vehicle control of BDCM) were used as control.

Mouse model for diet induced NASH

Pathogen-free, male, C57BL/6J background, wild type mice were fed with methionine and choline deficient (MCD) diet and were used as models for diet-induced NASH. Mice were fed with MCD diet from 8 to 12 weeks of age and livers harvested were used to study early stage of liver injury (MCD (4w)). Livers from mice fed with MCD diet from 8-16 weeks of age were used to study late stage of liver injury (MCD (8w)). Additionally, one set of wild type mice were fed with methionine and choline sufficient (MCS, control diet for MCD) were used as a control.

Administration of DETA NONOate, a nitric oxide donor (NO donor) and 1400W

DIO mice at 16 weeks were administered with BDCM and treated with DETA NONOate (1.0 mg/kg diluted in PBS) 1 h prior to each administration of BDCM, for 1 week (DIO+BDCM+NO (1w)) and for 4 weeks (DIO+BDCM+NO (4w)). MCD diet-fed mice were administered with DETA NONOate, twice in a week by intra-peritoneal route from

JPET Fast Forward. Published on October 27, 2014 as DOI: 10.1124/jpet.114.218131
This article has not been copyedited and formatted. The final version may differ from this version.

8-12 weeks of age (MCD+NO (4w)) and for 8-16 weeks of age (MCD+NO (8w)). 1400W was administered intraperitoneally as described previously(Chatterjee et al., 2012)

Inhibition of CYP2E1 by diallyl sulfide (CYP2E1 inhibitor)

Another set of MCD diet fed mice were treated with 50 mg/kg diallyl sulfide (diluted in corn oil), twice in a week by intra-peritoneal route from 8-12 weeks age of mice (MCD+DAS (4w)) and for 8-16 weeks age of mice (MCD+DAS (8w)(Hu et al., 1996).

Macrophage depletion by $GdCl_3$

DIO mice at 16 weeks were administered with BDCM and injected with gadolinium chloride $GdCl_3$ (10mg/kg) through the intravenous route 24 h prior to BDCM exposure(Chatterjee et al., 2012).

All mice had ad libitum access to food and water and were housed in a temperature-controlled room at 23-24°C with a 12-hour light/dark cycle. All animals were treated in strict accordance with the NIH Guide for the Humane Care and Use of Laboratory Animals and local IACUC standards. The study was approved by the institutional review board both at Duke University and the University of South Carolina at Columbia. After completion of the treatment, mice of all study groups were sacrificed for liver tissue and serum for the further experiments.

Immunohistochemistry

Formalin-fixed, paraffin-embedded liver tissue from all mice groups were cut into 5 µm thick tissue sections. Each section was deparaffinized using standard protocol as described by Seth RK et al (Seth et al., 2013). Epitope retrieval of deparaffinized sections was carried out using epitope retrieval solution and steamer (IHC-world,

Woodstock, MD) following manufacturer's protocol. Endogenous peroxidases were blocked using 3% H_2O_2 for 5 min. After blocking with 5% normal serum the tissue sections were incubated with primary antibodies (i) anti-4-Hydroxynonenal (ii) anti-α-smooth muscle actin (diluted as 1:500). Species-specific anti-IgG secondary antibodies and conjugation with HRP were performed using Vectastain Elite ABC kit (Vector Laboratories, Burlingame, CA) following manufacturer's protocols. 3,3' Diaminobenzedine (DAB) were used as a chromogen substrate. Sections were counter-stained with Mayer's hematoxylin. Washing with PBS-T was performed thrice between the steps. Sections were mounted in water based mounting media Simpo mount (GBI Labs, Mukilteo, WA) and observed under 10x/20x objective. Morphometric analysis was done using CellSens Software from Olympus America.

Immuno-fluorescence microscopy

Paraffin-embedded liver tissue from all the mouse groups was cut into 5 µm thick sections. Each section was deparaffinized using standard protocol. Heat based epitope retrieval of deparaffinized sections was carried out using epitope retrieval solution and steamer following manufacturer's protocol. The sections were treated with 0.01% triton X-100 before blocking with 5% normal serum. The primary antibodies (i) anti-IL-1β, (ii) anti-IL-12 and (iii) anti-IL-13 were used in 1:200 dilutions and incubated overnight at 4°C. Species-specific anti-IgG secondary antibody conjugated with Alexa Fluor 633 was used to observe the antigen specific immunoreactivity in red channel. Sections were mounted in ProLong gold antifade reagent with DAPI. Images were taken under 20x objectives using Olympus BX51 microscope.

Quantitative Real-Time Polymerase Chain Reaction (qRTPCR)

Gene expression levels in tissue samples were measured by two step qRTPCR. Standard protocol as described by Seth RK et al (Seth et al., 2013) was used to extract total RNA from liver tissue and to prepare cDNA from RNA extract. qRTPCR was performed with the gene specific forward and reverse primers using SsoAdvanced universal SYBR Green supermix (Bio-rad, Hercules, CA) and CFX96 thermal cycler (Bio-rad, Hercules, CA). Threshold Cycle (Ct) value for the selected genes were normalized against 18S (internal expression control) value in the same sample. Each reaction was carried out in triplicates for each gene and for each tissue sample. DIO mouse liver sample was used as the control for comparison with all other liver samples in the toxin-induced NASH group and MCS-diet fed mouse liver sample was used as control for comparison with all other liver samples of the diet-induced NASH group. The relative fold change was calculated by using CFX manager software. The sequences for the primers used for Real time PCR are provided below in 5' to 3' orientation:

Gene	***Primer sequence***
IL-1β	Sense: CCTCGGCCAAGACAGGTCGC Antisense: TGCCCATCAGAGGCAAGGAGGA
IL-12	Sense: GCTTCTCCCACAGGAGGTTT Antisense: CTAGACAAGGGCATGCTGGT
IL-23	Sense: AAAGGATCCGCCAAGGTCTG Antisense:GCAGGCTCCCCTTTGAAGAT
Dectin-1	Sense: AGGGAGCCACCTTCTCATCT Antisense: CTTCACCTTGGAGGCCCATT
IL-4	Sense:CATCGGCATTTTGAACGAG Antisense: CGAGCTCACTCTCTGTGGTG
IL-13	Sense: CACACAAGACCAGACTCCCC Antisense:TCTGGGTCCTGTAGATGGCA
CYP2E1	Sense: GGCGCATCGTGGTCCTGCAT Antisense: CCGCACGTCCTTCCATGTGGG
α-SMA	Sense: GGAGAAGCCCAGCCAGTCGC

	Antisense: ACCATTGTCGCACACCAGGGC

Western blot

25 mg of tissue from each liver sample was homogenized in 150 µl of RIPA buffer with protease inhibitor (1X) (Pierce, Rockford, IL) using dounce homogenizer. The homogenate was centrifuged; supernatant was collected and saved for experimental use. Denatured, 30 µg of protein from each homogenate was loaded per well of novex 4–12% bis-tris gradient gel (Life technologies, Carlsbad, CA) and subjected for SDS PAGE. Protein bands were transferred to nitrocellulose membrane using precut nitrocellulose/filter paper sandwiches (Bio-Rad, Hercules, CA) and Trans – Blot Turbo transfer system (Bio-Rad). Blots were blocked with 5% non-fat milk solution. Primary antibodies against CYP2E1 and β-actin were used at recommended dilutions. Species specific anti-IgG secondary antibody conjugated with HRP were used. Pierce ECL Western Blotting substrate (Thermo Fisher Scientific Inc., Rockford, IL) was used. The blot was developed using BioMax MS Films and cassettes (with intensifying screen, Kodak). The images were subjected to densitometry analysis using Lab Image 2006 Professional 1D gel analysis software from KAPLEAN Bioimaging Solutions, Liepzig, Germany.

Enzyme-linked immunosorbent assay (ELISA)

Immunoreactivity for 3-Nitrotyrosine was detected in liver homogenates using standard ELISA (Chatterjee S) (Chatterjee et al., 2009) (Chatterjee et al., 2009) (Chatterjee et al., 2009) (Chatterjee et al., 2009) (Chatterjee et al., 2009) (Chatterjee et al., 2009)

(Chatterjee et al., 2009) (Chatterjee et al., 2009) (Chatterjee et al., 2009). Briefly, polystyrene, high binding, 96 well plate coated with 5 µg of each protein. Wells were blocked with 5% non-fat milk. Primary antibody anti-3-Nitrotyrosine (1:1000 dilutions) was used. Species specific anti-IgG secondary antibody conjugated with HRP was used. TMB Substrate Solution (Pierce) was used to develop color. 2N sulfuric acid was used to stop the reaction. The plate was read at 450 nm using Synergy HT plate reader (BioTek Instruments, Inc., Winooski, VT). Immunoreactivity of HNE-His adduct was detected in liver homogenate using OxiSelect HNE-His adduct ELISA kit (Cell Biolabs, Inc. San Diego, CA) following manufacturer's protocol.

Histopathology

Formalin-fixed liver sections were stained with hematoxylin and eosin (H&E) as per standard protocol and observed under the light microscope using 10x objectives. Fibrotic stage of the liver tissue was evaluated by staining collagen deposition using Sirius red–staining of liver sections. Picro-Sirius red staining of liver sections was carried out by using Nova ultra sirius red stain kit following manufacturer's protocol (IHC world, Woodstock, MD).

Statistical Analyses

All *in vivo* experiments were repeated three times with 3 mice per group (N=3; data from each group of three mice were pooled). All experiments were repeated three times, and the statistical analysis was carried out by analysis of variance (ANOVA) including the morphometric analysis followed by the Bonferroni posthoc correction for intergroup comparisons. Quantitative data from mRNA expression as depicted by the relative fold

change were analyzed by performing a student's t test. For all analyzes P<0.05 was considered statistically significant.

Results:

Lipid peroxidation and tyrosyl radical formation in NASH progression is associated with the presence of hepatic CYP2E1. To study the nature of the oxidative species generated as a result of CYP2E1 activity in models of NASH, 4-HNE-Histidine (4-HNE-His) adducts and 3-Nitrotyrosine adducts were estimated by ELISA. Results showed that DIO+BDCM group had significantly increased 4-HNE-His adducts at 1 w post initiation of the study as compared to DIO group (*P<0.05)(Fig. 1A). Mice that were deficient in CYP2E1 gene had significantly decreased 4-HNE-His adducts as compared to DIO+BDCM group at the same time point (Fig. 1A). Since we used the toxin BDCM which is known to produce dihalomethyl radicals following its reactivity with CYP2E1, we used another commonly used dietary NASH model (Methionine and Choline deficient diet-fed mice) for evaluating the role of oxidative stress induced by CYP2E1. Results showed that 4-HNE-His adducts were significantly high in MCD group as compared to MCS control group at 4 w (comparable to 1 w of DIO model)(*P<0.05)(Fig. 1A). MCD diet-fed mice when treated with CYP2E1 inhibitor Diallyl sulfide (DAS) had significantly decreased 4-HNE-His adducts suggesting that CYP2E1 - is necessary for the generation of 4-HNE-His adducts, a direct consequence of lipid peroxidation in the liver (Fig. 1A). Earlier work with CYP2E1 suggested that the enzyme can produce superoxide radicals based on its strong NADPH oxidase like activity (Gergel et al., 1997). Similarly Gergel D et al have also shown that the O_2^- can react

with NO to produce $ONOO^{-}$ (Gergel et al., 1997). Based on its ability to produce $ONOO^{-}$, we studied the generation of 3-Nitrotyrosine adducts in - both toxin treated DIO mice and MCD diet-fed mice livers. Results showed that 3-Nitrotyrosine adduct levels were significantly increased in DIO+BDCM group as compared to only DIO group at 1 w(*P<0.05)(Fig. 1B). Absence of the CYP2E1 gene had significantly decreased 3-Nitrotyrosine adducts as compared to the DIO+BDCM group at the same time point (*P<0.05)(Fig. 1B). MCD diet-fed mice at 1 w had similar higher 3-Nitrotyrosine adducts as compared to control diet fed mice (*P<0.05), whereas MCD diet-fed mice that were treated with DAS had a significant decrease in the 3-Nitrotyrosine adduct formation (Fig. 1B), though a significant decrease in tyrosyl radical formation was not observed at 4w. The results suggested that CYP2E1 activity in NASH generates nitro-tyrosyl radicals probably through peroxynitrite formation from high CYP2E1-induced O_2^{-}at least in the diet+toxin model of NASH. It is interesting however that CYP2E1-induced 4-HNE can also generate O_2^{-}, thus producing tyrosyl radical formation and 3-Nitrotyrosine adducts (Whitsett et al., 2007).

Fig. 1C shows the localization of the immunoreactivity of 4-HNE in the livers of rodent NASH models. 4-HNE immunoreactivity was mainly localized in the Zone-3 (centrilobular) regions in the livers of BDCM model of NASH (Fig. 1C, i-iii), while the 4-HNE immunoreactivity was uniformly higher in centrolobular and periportal areas of livers from MCD-diet model of NASH. Absence of CYP2E1 enzyme (CYP2E1 KO) or administration of CYP2E1 inhibitor DAS significantly decreased the 4-HNE immunoreactivity in the NASH livers of both models (*P<0.05)(Fig. 1C and 1D). Nonavailability of a direct assay method that would only specifically estimate CYP2E1

activity from tissue homogenates led us to indirectly rely on the CYP2E1 induced oxidative radical formation as an index for assessing its catalytic role in the models of NASH being used in this study. BDCM is a hepatotoxin and is metabolized by CYP2E1 by forming dihalomethyl radicals as shown by Tomasi et al (Tomasi et al., 1985). Fig. 1E shows the illustrative example of the study and its rationale for measuring oxidative stress as an effective way to assess CYP2E1 activity.

CYP2E1-mediated oxidative stress is associated with M1 polarization bias in the NASH livers. Recent evidences involving morbidly obese patients that had NASH etiology were strongly associated with a specific increase in the liver expression of a wide array of proinflammatory M1 cytokines, especially IL-1β (Bertola et al., 2010). Recent reports from our laboratory has shown that CYP2E1 induced oxidative stress causes up regulation of pattern recognition receptor P2X7r which has a direct role in activation of Th1 cells (Das et al., 2013b). CYP2E1 null mice also had lower F4/80 positive cells which are primarily macrophages, followed by levels of intrahepatic TNF-α and MCP-1 as compared to wild type mice that had NASH (Abdelmegeed et al., 2012). To study the patterns of macrophage activation and M1 polarization bias in NASH we estimated the intrahepatic M1 cytokine levels of IL-1β, IL-12, IL-23 and Dectin-1. Since macrophages play a distinct role in the polarization, we administered macrophage toxin gadolinium chloride ($GdCl_3$) to deplete the residential and infiltrating macrophages in the liver, only in the toxin model of NASH to show the mechanistic role of the macrophages (Chatterjee et al., 2012). NASH develops over a period of time and is progressive in nature. An early phase of sinusoidal injury and inflammation is reported for most models

of NASH(Pasarin et al., 2012). For the toxin (DIO+BDCM) model of NASH, we used 1 was the time point for measuring M1 phenotypic shift and inflammation whereas we used 4 w for the MCD model since this model extends till 8 w. Results showed that mRNA expressions of IL-1β, IL-12, 1L-23 and Dectin-1 were significantly upregulated in the DIO+BDCM group as compared to DIO only group (*P<0.05)(Fig. 2A). CYP2E1 null mice or mice that were treated with $GdCl_3$ had significantly lower M1 cytokine levels as compared to DIO+BDCM group (*P<0.05)(Fig.2A). Similar trends were seen in the MCD model of NASH where IL-1β, IL-12, IL-23 and Dectin-1 mRNA were significantly up regulated in the early phase of NASH progression (4 weeks of MCD diet feeding) (*P<0.05)(Fig. 2B). To characterize the localization of M1 cytokines in the liver, immunofluorescence microscopy was performed on liver slices from both the toxin model and MCD-diet fed model of NASH. Results showed that IL-1β and IL-12 showed higher immunoreactivity in DIO+BDCM and MCD groups as compared to their respective controls (DIO and MCS) (Fig. 2C and 2D) while $GdCl_3$-treated and DAS-treated groups had significantly lower immunoreactivity for both IL-1β and IL-12. (Fig. 2C and 2D). Nitric oxide (NO) in the form of nitrite was measured from tissue homogenates (Fig. 2E). Results showed that the NO levels were significantly higher in DIO+BDCM group at 24 h, 1 w and 4 w while use of CYP2E1 null mice decreased the NO levels significantly (Fig. 2E). Use of 1400 W decreased the NO levels at 24 h. Use of NOS2 knockout mice did not significantly decrease the NO levels as compared to DIO+BDCM group, suggesting the involvement of other NOSs especially NOS3 (Fig. 2E). The above results clearly show that CYP2E1-induced oxidative stress might play a role in causingthe NASH liver to shift towards M1 type polarization bias. Further the the

decrease in NO levels folloin 1400W-treated (Specific NOS2 inhibitor) early phase of (24 h) NASH in mice and the resistance for a decrease following the use NOS2 KO mice at later stages show that there may be an involvement of other NOS2 in the early stage of NASH progression while other NOS isoforms, especially NOS3, probably from an adaptive response in the liver might contribute to the increased NO levels at the late stages of the disease.

M2 phenotypic cytokine release in late NASH stages are macrophage dependent. NASH is likely associated with a significantly prolonged anti-inflammatory phase which is predicted to originate from the initial M1 phase and can be shifted towards an M2 phenotype (Copaci et al., 2006). Several lines of evidence show that IL-10 and IL-13, IL-4 in some models of NASH have increased in late stages of NASH progression as reported by Shimamura et al (Shimamura et al., 2008). M2 cytokines, especially IL-4 and IL-13 were significantly elevated in a CCl_4-mediated fibrosis in liver, a feature that is linked to end stage NASH (Shimamura et al., 2008). To show later M2 polarization shift, we studied the M2 cytokine profiles in our models of NASH. Results showed that IL-4 and IL-13 were significantly elevated in mice that were co-exposed with the hepatotoxin BDCM and high fat diet (Fig. 3A)($P<0.001$). Interestingly, the mRNA levels of these cytokines were significantly down regulated in the MCD model of NASH (Fig. 3B). Depletion of macrophages by $GdCl_3$ significantly blunted the M2 phenotypic response (Fig. 3A)(*$P<0.05$), suggesting a direct link of the macrophage response in M2 phenotype bias. The above observation holds true since the M1 phenotypical response was also blunted in these mice following $GdCl_3$ administration. Surprisingly, IL-4 and IL-

13 mRNA expressions were significantly decreased in MCD model of NASH at 8 w (Fig. 3B). Interestingly IL-13 protein was significantly increased in both the models of NASH as evidenced by IL-13 immunoreactivity in the centrilobular areas of the liver in the toxin model and periportal regions of the MCD model (Fig. 3C). $GdCl_3$ administered liver slices showed decreased immunoreactivity to IL-13 suggesting the strong link ofM2 phenotypic shift in late stage NASH (4 weeks in cases of the toxin model and 8 weeks for MCD model of NASH (Fig. 3C).

Nitric Oxide donor administration attenuates CYP2E1-induced M1 cytokine production. Th1 polarization is an established phenomenon in early stage of NASH as is evidenced by both preclinical and clinical studies but there is sparse evidence of an M1 phenotype bias except for Kupffer cell M1/M2 transitions as reported by Maina V et al, Fukushima et al and Zhou D et al (Fukushima et al., 2009; Maina et al., 2012; Zhou et al., 2014). Having established the role of CYP2E1-induced M1 polarization bias in both toxin-induced high fat diet model and MCD model of NASH, we studied whether NO donor administration attenuated M1 polarization phenotype in both the models. The role of nitric oxide synthases (NOSs) and the generation of nitric oxide (NO) in the liver have not been studied with great detail. Not so recent studies by Fujita K et al show the direct involvement of NO in the development and progression of NASH (Fujita et al., 2010). They hypothesize based on the published studies that increased NO may be contributing to excess nitrotyrosine and hence increasing oxidative-nitosative stress in the liver (Fujita et al., 2010). In a recent report Ajamieh H et al reported that Atorvastatin conferred 70-90% hepatic protection in NASH (Ajamieh et al., 2012). The increased

expression of TLR4 and activation of NFkB was abrogated by the administration of atorvastatin which was found to activate endothelial nitric oxide synthase (eNOS/NOS3) (Ajamieh et al., 2012). Prevention and reversion of nonalcoholic steatohepatitis in ob/ob mice by S-nitroso-N-acetylcysteine treatment has been reported in leptin deficient mice (ob/ob) but there was no mechanistic insight about the protection seen (de Oliveira et al., 2008). Our own results as reported in Fig. 2E showed that increased NO response was not due to a proinflammatory NOS2-based response, and yet it can be justifiably assumed that it might be an adaptive response to liver injury. Based on the above evidence we studied the role of NO donor DETA NONOate on the corresponding M1 polarization-induced cytokine production and NASH progression. We attempted to study the early time points where we hypothesized polarization-induced cytokine induction to occur (1 w. for toxin model and 4 w. for MCD model). Results showed that mRNA levels of M1 markers IL-1β, IL-12, IL-23 and Dectin-1 were significantly decreased in NO donor administered group co-treated with high fat diet (HFD) and toxin BDCM (as a second hit) (Fig. 4A)(*P<0.05). Surprisingly MCD+NO donor group showed a significant increase in mRNA levels of the earlier described M1 markers as compared to only MCD group (Fig. 4B)(*P<0.05). Prominent M1 markers that had a significant increase in its mRNA patterns and based on their crucial roles in disease pathology namely IL-1β and IL-12 were then assessed for their protein levels and localization by immunofluorescence microscopy (Fig. 4C and 4D). Results showed that there was a visible decrease in IL-1β levels in NO donor groups of both models of NASH as compared to their respective BDCM treated or MCD diet-fed mice groups (Fig. 4C and 4D). The results suggested that there may be an interesting contrast between the

mRNA profiles of the M1 markers in both models but their protein profiles were found to be similar (decrease in M1 markers) following NO donor administration in both models of NASH.

Nitric Oxide donor administration attenuates M1 polarization via blockage of CYP2E1 protein-induced oxidative stress. Pioneering studies by Gergel D et al showed that nitric oxide could inhibit CYP2E1 activity and oxygen radical formation (Gergel et al., 1997). The liver-selective nitric oxide donor O2-vinyl 1-(pyrrolidin-1-yl)diazen-1-ium-1,2-diolate (V-PYRRO/NO) protects HepG2 cells against cytochrome P450 2E1-dependent toxicity (Gong et al., 2004). Based on this strong argument, we studied the mechanism of attenuation of M1 polarization by DETA NONOate. Results showed that administration of NO donor significantly decreased the mRNA levels of CYP2E1 at 1 week. post co-treatment with toxin and high fat diet (termed as the initial phase) as compared to DIO+BDCM group alone (*P<0.05)(Fig.5A). Surprisingly the mRNA levels of CYP2E1 was increased significantly in the MCD model of NASH following NO donor administration (Fig. 5B)(*P<0.05). Western blot analysis of the CYP2E1 protein showed no significant change in the liver levels of the protein in either of the two models except in CYP2E1 null mice (Fig. 5C). Since NO donor has been shown to inhibit CYP2E1 activity and we could not identify a direct assay system to quantify CYP2E1 activity from liver homogenates, we resorted to the CYP2E1 induced lipid peroxidation as an index of CYP2E1 activity. ELISA and immunohistochemistry was used to quantify the lipid peroxidation product 4-HNE-His adducts following NO donor administration. Results showed that there was a significant decrease in 4-HNE-

His adducts in NO donor administered group as compared to DIO+BDCM group at 1 week post study initiation, a time point where both increased oxidative stress and M1 polarization were observed (Fig. 5D) (*P<0.05). This result was also observed in MCD model of NASH co-administered with NO donor. NO donor group of MCD diet fed mice had significant decrease in 4-HNE-His adducts as compared to MCD group (Fig. 5D)(*P<0.05). Immunoreactivity to 4-HNE the lipid peroxidation product was also significantly decreased in NO donor group for both the BDCM model and the MCD model of NASH (Fig. 5E and 5F)(*P<0.05). The results strongly suggested that NO donor administration significantly decreased CYP2E1 induced oxidative stress which has been shown to be directly correlated to M1 polarization and NASH progression. The above conclusions are strengthened by supplemental data for serum ALT and HMGB1 mrna expressions. Results showed that serum ALT levels and HMGB1 mrna expression were significantly decreased in NO donor administered groups as compared to MCD or DIO+BDCM group (Supplemental Figs. 1 and 2) suggesting that the a marked decrease in CYP2E1 activity following NO donor administration decreases the bioactivation of BDCM and toxicity in MCD group.

Nitric Oxide donor administration rescues mice from NASH progression. NASH progression is marked by a proinflammatory stage followed mostly by a fibrotic stage (Farrell and Larter, 2006; Bohinc and Diehl, 2012). Hepatic stellate cells transform into a more activated and proliferative phenotype (Mann and Marra, 2010; Bohinc and Diehl, 2012). There is increased collagen deposition and buildup of extracellular matrix. If unchecked, this phenomenon can lead to scarring of the liver and ultimately can lead to

liver cirrhosis (Ikejima et al., 2007). To study whether attenuation of M1 polarization by NO donor administration also rescued the livers from progressive NASH phenotype, experiments were performed in both models of NASH to study stellate cell proliferation, collagen deposition and histopathological examination of the affected livers by following the NASH CRN scoring system. Results showed that administration of NO donor in both models of NASH significantly decreased the mRNA expression of α-smooth muscle actin (α-SMA), a biomarker for stellate cell proliferation (Fig. 6A and 6B)(*$P<0.05$). Immunohistochemistry of liver slices from both the toxin model and MCD models of NASH showed significant increased immunoreactivity of α-SMA in sinusoidal regions in BDCM treated NASH mice and MCD diet-fed mice (Fig. 6C i and iii) while there was a decreased immunoreactivity for α-SMA in NO donor treated mice livers that were either on toxin administered group or in MCD diet group (Fig. 6C ii and iv). Picro Sirius red staining for collagen deposition in the livers showed higher periportal fibrosis in both the toxin treated mice and MCD diet-fed mice while fibrosis was markedly reduced in the NO donor treated mice (Fig. 6D). Liver histology as evidenced by hematoxylin and eosin staining showed decreased bipolar nuclei, infiltrating leukocytes, ballooning degeneration and hepatocyte necrosis in NO donor groups as compared to BDCM treated group (Fig. 6E). NASH CRN scores showed a significant attenuation of severity of NASH lesions as described in the NASH CRN scores (Fig. 6F). The results thus suggest that NO donor administration could significantly rescue mice from NASH lesions following NO donor administration through their entire period of high fat diet and toxin exposure or MCD diet feeding. A schematic representation of the NO-donor mechanism of action is provided in Fig. 7.

Discussion: In this study we report for the first time, a mechanistic investigation of oxidative stress-induced M1 polarization, evidenced by M1 cytokine release in NASH followed by a therapeutic intervention of the said process by NO-donor utilizing its inhibitory effect on CYP2E1, a vital enzyme with a recognized role in NASH progression. Our study found that lipid peroxidation-induced 4-HNE-histidine adducts that were generated from CYP2E1 catalysis of BDCM in the toxin model of NASH and dietary oxidative stress in MCD model of NASH caused M1 polarization bias-induced cytokine release that included increased levels of hepatic M1 markers namely, IL-1β, IL-12, IL-23 and Dectin-1. We used two distinct models of NASH progression in mice, firstly using a specific ligand of CYP2E1 (BDCM) in an underlying condition of obesity (high fat diet) and insulin resistance, and secondly a dietary model (MCD) where the mice progress into steatohepatitis and fibrosis amidst oxidative stress especially through CYP2E1 without obesity and insulin resistance. The use of these two separate mouse models justified our approach to probe the involvement of oxidative stress M1 polarization-induced cytokine release without having to limit our interpretation based on a single dietary model of NASH. We have shown previously that BDCM exposure to high fat diet fed mice causes NASH (Das et al., 2013a; Seth et al., 2013). These mice had an increased proinflammatory cytokine release (1 w.) followed by a progressive fibrotic stage (up to 4 w.). The increased proinflammatory phase was primarily because of the involvement of CYP2E1 mediated oxidative stress and inflammosome activation due to priming of the P2X7r (Das et al., 2013b). Th1 polarization in NASH has been studied in details (Ferreyra Solari et al., 2012; Maina et al., 2012; Sutti et al., 2014). The

JPET Fast Forward. Published on October 27, 2014 as DOI: 10.1124/jpet.114.218131
This article has not been copyedited and formatted. The final version may differ from this version.

higher incidences of IFN-γ release is primarily from a heightened Th1 response and is found to be due to oxidative stress mediated malonyldialdehyde (MDA) adducts that elicit a strong autoantibody response (Sutti et al., 2014). The adaptive immune response then is responsible for macrophage polarization mainly through M1 phenotype (Sutti et al., 2014). Our observation of decreased hepatic M1 markers in CYP2E1 null mice and in mice treated with CYP2E1 inhibitor DAS in both models of NASH show a close association of CYP2E1-induced oxidative stress in causing M1 polarization bias and increase in the M1 markers. Importantly our approach to deplete macrophages by using $GdCl_3$ in the liver was based on identifying the precise origin of the inflammatory cytokines, especially IL-1β, IL-12, IL-23 and Dectin-1 being well aware of the fact that IL1β release also has other cellular sources in the liver. Our results of CYP2E1 mediated M1 polarization in NASH provides insights into the mechanisms of macrophage responses which has been scarce except for a few isolated studies where morbidly obese patients with NASH etiology has been shown to produce increased Th1 cytokines and Kupffer cell responses (Fukushima et al., 2009; Bertola et al., 2010; Bieghs et al., 2013). Several preclinical evidences suggest the involvement of Kupffer cells with an M1 phenotype, the former being responsible for NASH progression, however these studies do not clarify the role of oxidative stress, especially mediated by CYP2E1 in causing a M1 polarization bias (Fukushima et al., 2009; Bieghs et al., 2013). Important from the mechanistic point of view, we observed an increase in the hepatic nitric oxide levels in the diet+toxin NASH model. Nitric oxide, released from any of the three nitric oxide synthases upon their activation play significant roles in inflammation (Fujita et al., 2010; Ajamieh et al., 2012). However, inducible form of the NO synthase

has been ascribed to the proinflammatory phenotype more often (Fujita et al., 2010; Maina et al., 2012). Results from our study showed that NO levels reached a 4 fold increase as early as 24 h following co-exposure with diet and toxin to induce NASH and stayed at the same level for the entire study period. Early use of 1400W decreased NO levels. Interestingly use of NOS2 null mice at a late stage (4 wk) did not affect the NO levels in NASH, suggesting that other NOS isoforms, especially NOS3 might be involved in the sustained higher NO levels at a late stage found in our study. Moreover in the observed increase in NO may be an adaptive response of the injured liver. Recent report by Ajamieh H et al found that there were increases in NOS3 levels and NOS3 phosphorylations following liver injury in NASH and were found to be protective against NASH (Ajamieh et al., 2012). Based on the observations, we argued that though NO is considered proinflammatory and an M1 marker, the kinetics of NO release and its concentration in the hepatic microenvironment might play an adaptive and perhaps a protective role in the pathophysiology of NASH. To alter the NO levels we used a dual approach. We used NOS2 null mice and a nonspecific inhibitor of NOS. Subsequently we used an NO donor DETA NONOate for administration through the IP route to increase the in vivo concentration of NO assuming that the increase in NO was an adaptive response to the liver injury. While blocking NO synthase did not change levels of M1 polarization markers and NASH symptoms (data not shown), treatment with NO donor significantly lowered levels of both mRNA and protein expressions of M1 markers in the toxin model while only protein levels in the MCD model of NASH (Fig. 4A-D) suggesting an existence of a plausible mechanism for NO mediated suppression of proinflammatory events in early NASH developmental stages.

Having identified an association of CYP2E1-induced oxidative stress as a mediator in M1 polarization, we studied the role of a late M2 phenotype that might aid to cause fibrosis, a feature that is of paramount importance in the human form of the disease. Results from our studies showed that mice from the high fat diet-induced obesity and co-exposed to the toxin BDCM had increased mRNA and protein expressions of both IL-4 and IL-13, prominent M2 markers whereas mice that were pretreated with macrophage toxin $GdCl_3$ did not show the increases in both IL-4 and IL-13 suggesting that the a macrophage origin contributed at least partly to the M2 phenotypic shift in the late stage of the disease. Since NO donor prevented M1 polarization bias, we also argued that a higher NO concentration from the initial phases of the disease development might resist the proinflammatory events in early stages of NASH, with a corresponding decrease in M2 phenotypic response thus attenuating NASH progression.

Since M1 polarization was associated with CYP2E1 mediated oxidative stress and CYP2E1 activity is strongly inhibited by NO, we studied the role of NO donor (DETA NONOate) in abrogating the oxidative stress, mediated by CYP2E1 activity. Our results of a strong inhibition of 4-HNE-Histidine adducts in both the models of NASH was in complete agreement with the pioneering study by Gergel D et al, who showed that CYP2E1 catalytic activity and reactive oxygen radical formation was inhibited by NO (Fig. 5) (Gergel et al., 1997). Our observations that there was no change in CYP2E1 protein level following NO donor administration also confirmed that NO donor inhibited CYP2E1 activity in the in vivo system that we have used for our study.

NASH pathophysiology is associated with stellate cell proliferation, fibrosis and hepatocellular necrosis (Bohinc and Diehl, 2012; Seth et al., 2013). NO donor administration significantly decreased stellate cell proliferation as evidenced by decreased α-SMA protein levels, caused decreased hepatocellular necrosis, inflammation and fibrosis as shown by NASH CRN scores (Fig. 6). Thus taken together, this study showed that oxidative stress mediated by CYP2E1 induced M1 polarization-induced cytokines which in turn might have been responsible for late anti-inflammatory events that resulted in fibrosis. Mechanistically, administration of NO donor that increased the NO levels in the liver significantly (6.6 fold as compared to 3.4 fold, data not shown) could block CYP2E1 activity and subsequent inflammatory events that lead to NASH pathophysiology. The study offers a therapeutic approach through use of NO donors as prospective drugs for NASH treatment and leads the way for a much detailed insight into developing newer and effective pharmacological strategies involving synthetic NO donors with longer half-lives to contain NASH related co-morbidities.

Acknowledgements: The authors gratefully acknowledge the technical services of Benny Davidson at the IRF, University of South Carolina School of Medicine. We also thank Dr. James Carson, Department of Exercise Science and the Instrumentation resource facility (IRF) at the University of South Carolina for equipment usage and consulting services.

Authorship Contributions:
Participated in research design: Chatterjee, Seth
Conducted experiments: Seth, Das, Pourhosseini, Dattaroy, Igwe
Contributed new reagents or analytic tools: Diehl, Michelotti
Performed data analysis: Chatterjee, Das, Seth
Wrote or contributed to the writing of the manuscript: Chatterjee, Fan, Diehl, Basu-Ray, Michelotti.

References:

Abdelmegeed MA, Banerjee A, Jang S, Yoo SH, Yun JW, Gonzalez FJ, Keshavarzian A and Song BJ (2013) CYP2E1 potentiates binge alcohol-induced gut leakiness, steatohepatitis, and apoptosis. *Free Radic Biol Med* **65**:1238-1245.

Abdelmegeed MA, Banerjee A, Yoo SH, Jang S, Gonzalez FJ and Song BJ (2012) Critical role of cytochrome P450 2E1 (CYP2E1) in the development of high fat-induced non-alcoholic steatohepatitis. *J Hepatol* **57**:860-866.

Aitken AE, Lee CM and Morgan ET (2008) Roles of nitric oxide in inflammatory downregulation of human cytochromes P450. *Free Radic Biol Med* **44**:1161-1168.

Ajamieh H, Farrell G, Wong HJ, Yu J, Chu E, Chen J and Teoh N (2012) Atorvastatin protects obese mice against hepatic ischemia-reperfusion injury by Toll-like receptor-4 suppression and endothelial nitric oxide synthase activation. *Journal of gastroenterology and hepatology* **27**:1353-1361.

Aubert J, Begriche K, Knockaert L, Robin MA and Fromenty B (2011) Increased expression of cytochrome P450 2E1 in nonalcoholic fatty liver disease: mechanisms and pathophysiological role. *Clinics and research in hepatology and gastroenterology* **35**:630-637.

Bertola A, Bonnafous S, Anty R, Patouraux S, Saint-Paul MC, Iannelli A, Gugenheim J, Barr J, Mato JM, Le Marchand-Brustel Y, Tran A and Gual P (2010) Hepatic expression patterns of inflammatory and immune response genes associated with obesity and NASH in morbidly obese patients. *PloS one* **5**:e13577.

Bieghs V, Walenbergh SM, Hendrikx T, van Gorp PJ, Verheyen F, Olde Damink SW, Masclee AA, Koek GH, Hofker MH, Binder CJ and Shiri-Sverdlov R (2013) Trapping of oxidized LDL in lysosomes of Kupffer cells is a trigger for hepatic inflammation. *Liver international : official journal of the International Association for the Study of the Liver* **33**:1056-1061.

Bohinc BN and Diehl AM (2012) Mechanisms of disease progression in NASH: new paradigms. *Clinics in liver disease* **16**:549-565.

Caro AA and Cederbaum AI (2004) Oxidative stress, toxicology, and pharmacology of CYP2E1. *Annual review of pharmacology and toxicology* **44**:27-42.

Chatterjee S, Ehrenshaft M, Bhattacharjee S, Deterding LJ, Bonini MG, Corbett J, Kadiiska MB, Tomer KB and Mason RP (2009) Immuno-spin trapping of a post-translational carboxypeptidase B1 radical formed by a dual role of xanthine oxidase and endothelial nitric oxide synthase in acute septic mice. *Free Radic Biol Med* **46**:454-461.

Chatterjee S, Ganini D, Tokar EJ, Kumar A, Das S, Corbett J, Kadiiska M, Waalkes M, Diehl AM and Mason RP (2012) Leptin is key to peroxynitrite-mediated oxidative stress and Kupffer cell activation in experimental nonalcoholic steatohepatitis. *J Hepatol*.

Chatterjee S, Premachandran S, Bagewadikar RS, Bhattacharya S, Chattopadhyay S and Poduval TB (2006) Arginine metabolic pathways determine its therapeutic benefit in experimental heatstroke: role of Th1/Th2 cytokine balance. *Nitric oxide : biology and chemistry / official journal of the Nitric Oxide Society* **15**:408-416.

Cheung O and Sanyal AJ (2009) Recent advances in nonalcoholic fatty liver disease. *Current opinion in gastroenterology* **25**:230-237.

Copaci I, Micu L and Voiculescu M (2006) The role of cytokines in non-alcoholic steatohepatitis. A review. *Journal of gastrointestinal and liver diseases : JGLD* **15**:363-373.

Das S, Kumar A, Seth RK, Tokar EJ, Kadiiska MB, Waalkes MP, Mason RP and Chatterjee S (2013a) Proinflammatory adipokine leptin mediates disinfection byproduct bromodichloromethane-induced early steatohepatitic injury in obesity. *Toxicology and applied pharmacology*.

Das S, Seth RK, Kumar A, Kadiiska MB, Michelotti G, Diehl AM and Chatterjee S (2013b) Purinergic receptor X7 is a key modulator of metabolic oxidative stress-mediated autophagy and inflammation in experimental nonalcoholic steatohepatitis. *American journal of physiology Gastrointestinal and liver physiology* **305**:G950-963.

de Oliveira CP, de Lima VM, Simplicio FI, Soriano FG, de Mello ES, de Souza HP, Alves VA, Laurindo FR, Carrilho FJ and de Oliveira MG (2008) Prevention and reversion of nonalcoholic steatohepatitis in OB/OB mice by S-nitroso-N-acetylcysteine treatment. *Journal of the American College of Nutrition* **27**:299-305.

Farrell GC and Larter CZ (2006) Nonalcoholic fatty liver disease: from steatosis to cirrhosis. *Hepatology* **43**:S99-S112.

Ferreyra Solari NE, Inzaugarat ME, Baz P, De Matteo E, Lezama C, Galoppo M, Galoppo C and Chernavsky AC (2012) The role of innate cells is coupled to a Th1-polarized immune response in pediatric nonalcoholic steatohepatitis. *Journal of clinical immunology* **32**:611-621.

Fujita K, Nozaki Y, Yoneda M, Wada K, Takahashi H, Kirikoshi H, Inamori M, Saito S, Iwasaki T, Terauchi Y, Maeyama S and Nakajima A (2010) Nitric oxide plays a crucial role in the development/progression of nonalcoholic steatohepatitis in the choline-deficient, l-amino acid-defined diet-fed rat model. *Alcoholism, clinical and experimental research* **34 Suppl 1**:S18-24.

Fukushima J, Kamada Y, Matsumoto H, Yoshida Y, Ezaki H, Takemura T, Saji Y, Igura T, Tsutsui S, Kihara S, Funahashi T, Shimomura I, Tamura S, Kiso S and Hayashi N (2009) Adiponectin prevents progression of steatohepatitis in mice by regulating oxidative stress and Kupffer cell phenotype polarization. *Hepatology research : the official journal of the Japan Society of Hepatology* **39**:724-738.

Ganz M and Szabo G (2013) Immune and inflammatory pathways in NASH. *Hepatology international* **7**:771-781.

Gergel D, Misik V, Riesz P and Cederbaum AI (1997) Inhibition of rat and human cytochrome P4502E1 catalytic activity and reactive oxygen radical formation by nitric oxide. *Archives of biochemistry and biophysics* **337**:239-250.

Gong P, Cederbaum AI and Nieto N (2004) The liver-selective nitric oxide donor O2-vinyl 1-(pyrrolidin-1-yl)diazen-1-ium-1,2-diolate (V-PYRRO/NO) protects HepG2 cells against cytochrome P450 2E1-dependent toxicity. *Molecular pharmacology* **65**:130-138.

Hu JJ, Yoo JS, Lin M, Wang EJ and Yang CS (1996) Protective effects of diallyl sulfide on acetaminophen-induced toxicities. *Food and chemical toxicology : an international journal published for the British Industrial Biological Research Association* **34**:963-969.

Ikejima K, Okumura K, Kon K, Takei Y and Sato N (2007) Role of adipocytokines in hepatic fibrogenesis. *Journal of gastroenterology and hepatology* **22 Suppl 1**:S87-92.

Liu YC, Zou XB, Chai YF and Yao YM (2014) Macrophage Polarization in Inflammatory Diseases. *International journal of biological sciences* **10**:520-529.

Maina V, Sutti S, Locatelli I, Vidali M, Mombello C, Bozzola C and Albano E (2012) Bias in macrophage activation pattern influences non-alcoholic steatohepatitis (NASH) in mice. *Clinical science (London, England : 1979)* **122**:545-553.

Mann DA and Marra F (2010) Fibrogenic signalling in hepatic stellate cells. *J Hepatol* **52**:949-950.

Pasarin M, La Mura V, Gracia-Sancho J, Garcia-Caldero H, Rodriguez-Vilarrupla A, Garcia-Pagan JC, Bosch J and Abraldes JG (2012) Sinusoidal endothelial dysfunction precedes inflammation and fibrosis in a model of NAFLD. *PloS one* **7**:e32785.

Seth RK, Das S, Kumar A, Chanda A, Kadiiska MB, Michelotti G, Manautou J, Diehl AM and Chatterjee S (2014) CYP2E1-dependent and leptin-mediated hepatic CD57 expression on CD8+ T cells aid progression of environment-linked nonalcoholic steatohepatitis. *Toxicology and applied pharmacology* **274**:42-54.

Seth RK, Kumar A, Das S, Kadiiska MB, Michelotti G, Diehl AM and Chatterjee S (2013) Environmental toxin-linked nonalcoholic steatohepatitis and hepatic metabolic reprogramming in obese mice. *Toxicological sciences : an official journal of the Society of Toxicology*.

Shimamura T, Fujisawa T, Husain SR, Kioi M, Nakajima A and Puri RK (2008) Novel role of IL-13 in fibrosis induced by nonalcoholic steatohepatitis and its amelioration by IL-13R-directed cytotoxin in a rat model. *J Immunol* **181**:4656-4665.

Sutti S, Jindal A, Locatelli I, Vacchiano M, Gigliotti L, Bozzola C and Albano E (2014) Adaptive immune responses triggered by oxidative stress contribute to hepatic inflammation in NASH. *Hepatology* **59**:886-897.

Tilg H and Moschen AR (2008) Inflammatory mechanisms in the regulation of insulin resistance. *Molecular medicine (Cambridge, Mass)* **14**:222-231.

Tilg H and Moschen AR (2010) Evolution of inflammation in nonalcoholic fatty liver disease: the multiple parallel hits hypothesis. *Hepatology* **52**:1836-1846.

Tomasi A, Albano E, Biasi F, Slater TF, Vannini V and Dianzani MU (1985) Activation of chloroform and related trihalomethanes to free radical intermediates in isolated hepatocytes and in the rat in vivo as detected by the ESR-spin trapping technique. *Chemico-biological interactions* **55**:303-316.

Whitsett J, Picklo MJ, Sr. and Vasquez-Vivar J (2007) 4-Hydroxy-2-nonenal increases superoxide anion radical in endothelial cells via stimulated GTP cyclohydrolase proteasomal degradation. *Arteriosclerosis, thrombosis, and vascular biology* **27**:2340-2347.

Zhou D, Kong L, Zhou Q and Li J (2014) Skewing KC phenotypic polarization into M2 via the intervention of oxidized LDL as potential therapeutic implications for NASH. *Liver international : official journal of the International Association for the Study of the Liver* **34**:815-816.

Footnotes:

This work has been supported by National Institutes of Health pathway to Independence Award, NIH R00 [4R00ES019875-02 to Saurabh Chatterjee], NIH R01 [R01DK053792 to Anna Mae Diehl] and the Intramural Research Program of the National Institutes of Health and the National Institute of Environmental Health Sciences.

JPET Fast Forward. Published on October 27, 2014 as DOI: 10.1124/jpet.114.218131
This article has not been copyedited and formatted. The final version may differ from this version.

Figure Legends:

Fig. 1. BDCM exposure in diet induced obese (DIO) mice and methionine and choline deficient (MCD) diet in wild type mice generates CYP2E1-mediated oxidative stress. A. Quantification of 4-HNE-His adducts (stable adducts of 4-hydroxynonenal (4-HNE)) in mouse liver homogenate by indirect ELISA of DIO, DIO mice exposed with bromodichloromethane (BDCM) for 1 week (DIO+BDCM (1w)), CYP2E1 gene deleted mice exposed to BDCM (CYP2E1 KO), methionine and choline sufficient diet fed mice (MCS), methionine and choline deficient diet fed mice (MCD) and MCD diet fed mice treated with diallyl disulfide (CYP2E1 inhibitor) for 4 weeks (MCD+DAS). Y-axis represents pg/mL of 4-HNE-His adduct (n=3). $P<0.05$ is considered statistically significant (*). **B.** Indirect ELISA of 3-Nitrotyrosine in mouse liver homogenate of DIO, DIO+BDCM (1w), CYP2E1 KO, MCS, MCD and MCD+DAS (1 w and 4 w). Y-axis represents the % levels of 3-Nitrotyrosine immunoreactivity, n=3. $P<0.05$ is considered statistically significant (*). **C.** Immunohistochemistry of mouse liver slices depicting 4-HNE immunoreactivity (lipid peroxidation) in DIO, DIO+BDCM (1w), CYP2E1 KO, MCS, MCD and MCD+DAS. (n=3), 10x image. **D.** Morphometric analysis of 4-HNE immunoreactivity. Y-axis shows % positive immunoreactive area. (n=3, analysis done on images from three separate microscopic fields). $P<0.05$ is considered statistically significant (*).

Fig. 2. M1 polarization depends on oxidative stress mediated by CYP2E1 activity. A. qRTPCR analysis of liver IL-1β, IL-12, IL-23 and Dectin-1 mRNA expression of DIO, DIO+BDCM (1w), CYP2E1KO and $GdCl_3$ treated (macrophage depleted) mice. Y-axis represents fold of mRNA expression when normalized against DIO only group, n=3. $P<0.05$ is considered statistically significant (*). **B.** qRTPCR analysis of liver IL-1β, IL-12, IL-23 and Dectin-1 mRNA expression of MCS and MCD diet fed mice. Y-axis represents fold of mRNA expression when normalized against MCS only group, n=3. $P<0.05$ is considered statistically significant (*). **C.** Immunofluorescence images of IL-1β immunoreactivity (red), counter stained with DAPI (blue) of paraffin embedded liver sections from DIO (i), DIO+BDCM (1w) (ii), CYP2E1KO (iii), $GdCl_3$ (iv), MCS (v), MCD (vi), MCD+DAS (vii). 20x magnification, n=3. **D.** Immunofluorescence images of IL-12

immunoreactivity (red), counter stained with DAPI (blue) of paraffin embedded liver sections from DIO (i), DIO+BDCM (1w) (ii), CYP2E1KO (iii), $GdCl_3$ (iv), MCS (v), MCD (vi), MCD+DAS (vii). 20X magnification, n=3. **E.** Nitric oxide (NO) levels measured as total nitrite (nitrite and nitrate converted to nitrite) by fluorometric assay in liver homogenates of DIO, DIO mice exposed to BDCM for 24 h (DIO+BDCM, 24 h), for 48h (DIO+BDCM, 48h), for 1 week (DIO+BDCM, 1w), for 4 weeks (DIO+BDCM, 4w) and nitric oxide synthase 2 (inducible) gene deleted mice and 1400W administered mice (1400W) exposed to BDCM 24 h and for 4 weeks (NOS2 KO+BDCM, 4w). Y-axis represents fold of NO levels when normalized against DIO only group, n=3. $P<0.05$ is considered statistically significant (*).

Fig. 3. Chronic exposure of BDCM leads to late M2 phenotypic shift. A. qRTPCR analysis of liver IL-4 and IL-13 mRNA expression of DIO, DIO+BDCM (4w) and $GdCl_3$ treated mice. Y-axis represents fold of mRNA expression when normalized against DIO only group, n=3. $P<0.05$ is considered statistically significant (*). **B.** qRTPCR analysis of liver IL-4 and IL-13 mRNA expression of MCS and MCD diet fed mice. Y-axis represents fold of mRNA expression when normalized against MCS only group, n=3. $P<0.05$ is considered statistically significant (*). **C.** Immunofluorescence images of IL-13 immunoreactivity (red), counter stained with DAPI (blue) of paraffin embedded liver sections from DIO (i), DIO+BDCM (4w) (ii), $GdCl_3$ (iii), MCS (iv), MCD (v). 20x magnification, n=3.

Fig. 4. NO donor DETA NONOate attenuates the CYP2E1-mediated M1 polarization bias. A. mRNA expression analysis by qRTPCR of liver IL-1β, IL-12, IL-23 and Dectin-1 of DIO, DIO+BDCM (1w) and DIO mice exposed with BDCM and treated with DETA NONOate for 1 week (DIO+BDCM+NO (1w)). Y-axis represents fold of mRNA expression when normalized against DIO only group, n=3. $P<0.05$ is considered statistically significant (*). **B.** qRTPCR analysis of liver IL-1β, IL-12, IL-23 and Dectin-1 mRNA expression of MCS, MCD and MCD mice treated with DETA NONOate for 4 weeks (MCD+NO). Y-axis represents fold of mRNA expression when normalized against MCS only group, n=3. $P<0.05$ is considered statistically significant (*). **C.** Analysis of IL-1β immunoreactivity (red) by immunofluorescence imaging of paraffin

embedded liver sections, counter stained with DAPI (blue) from DIO (i), DIO+BDCM (1w) (ii), DIO+BDCM+NO (iii), MCS (iv), MCD (v) and MCD+NO (vi). 20x magnification, n=3. **D.** Immunofluorescence images of IL-12 immunoreactivity (red) of paraffin embedded liver sections counter stained with DAPI (blue) from DIO (i), DIO+BDCM (1w) (ii), DIO+BDCM+NO (iii), MCS (iv), MCD (v) and MCD+NO (vi). 20x magnification, n=3.

Fig. 5. NO donor (DETA NONOate) decreases oxidative stress by inhibiting CYP2E1 activity. A. mRNA expression analysis of liver CYP2E1 by qRTPCR of DIO+BDCM (1w) and DIO mice exposed with BDCM and treated with DETA NONOate for 1 week (DIO+BDCM+NO (1w). Y-axis represents fold of mRNA expression when normalized against DIO only group, n=3. $P<0.05$ is considered statistically significant (*). **B.** qRTPCR analysis of liver CYP2E1 mRNA expression of MCD and MCD mice treated with DETA NONOate 4weeks (MCD+NO). Y-axis represents fold of mRNA expression when normalized against MCS only group, n=3. $P<0.05$ is considered statistically significant (*). **C.** Western Blot analysis of CYP2E1 protein expression levels in liver homogenates from DIO, DIO+BDCM (1w), CYP2E1KO, MCS, MCD, MCD+DAS and DIO+BDCM (1w), DIO+BDCM+NO (1w), MCD(4w), MCD+NO(4w) mice. The corresponding β-actin levels are shown in the lower panel. **D.** Quantification of HNE-His adduct in mouse liver homogenate by indirect ELISA of DIO+BDCM (1w), DIO+BDCM+NO (1w), MCD(4w) and MCD+NO(4w) mice. Y-axis represents pg/mL of HNE-His adduct (n=3). $P<0.05$ is considered statistically significant (*). **E.** 4-HNE immunoreactivity analysis of mouse liver slices by Immunohistochemistry depicting lipid peroxidation in DIO+BDCM (1w), DIO+BDCM+NO (1w), MCD (4w) and MCD+NO (4w) mice. (n=3), 10x image. **F.** Morphometric analysis of 4-HNE immunoreactivity. Y-axis shows % positive immunoreactive area. (n=3, analysis done on images from three separate microscopic fields). $P<0.05$ is considered statistically significant (*).

Fig. 6. NO donor (DETA NONOate) prevents NASH progression by inhibiting CYP2E1 activity and the resultant oxidative stress. A. mRNA expression of liver α-Smooth muscle actin (α-SMA) by qRTPCR of DIO mice exposed with BDCM for 4 weeks (DIO+BDCM (4w)) and DIO+BDCM mice treated with NO donor for 4 weeks (DIO+BDCM+NO (4w)). Y-axis represents fold of mRNA expression when normalized

against DIO only group, n=3. P<0.05 is considered statistically significant (*). **B.** qRTPCR analysis of liver α-SMA mRNA expression of MCD mice and MCD mice treated with DETA NONOate 4weeks (MCD+NO).Y-axis represents fold of mRNA expression when normalized against MCS only group, n=3. P<0.05 is considered statistically significant (*). **C.** α-smooth muscle actin immunoreactivity as shown by immunohistochemistry in liver slices of DIO mice exposed with BDCM (i), DIO+BDCM mice treated with NO donor (ii), MCD mice (iii) and MCD mice treated with NO donor (iv) 20x images (n=3) . **D.** Picro sirius red staining of liver sections of DIO mice exposed with BDCM (i), DIO mice exposed BDCM and treated with NO donor (ii), MCD mice (iii) and MCD mice treated with NO donor (iv) 20x images (n=3). Red staining depicts macro and micro vesicular fibrosis. **E.** Hematoxylin and Eosin staining of liver sections of DIO mice exposed with BDCM (i), DIO mice exposed BDCM and treated with NO donor (ii), MCD mice (iii) and MCD mice treated with NO donor (iv) 10x images (n=3). **F.** Stained liver sections were reviewed for stages of fibrosis using the criteria of the NIH Non Alcoholic Steatohepatitis Clinical Research Network (NIH NASH CRN). Table depicts the NASH CRN scores for DIO, DIO+BDCM, DIO+BDCM+NO, MCS, MCD and MCD+NO mice.

Fig. 7. Schematic representation of the study: The graphical scheme represents the proposed mechanism of action of DETA NO NOate. The checkpoints where the drug can have its potential inhibitory role are represented in red lines.

Fig. 1.

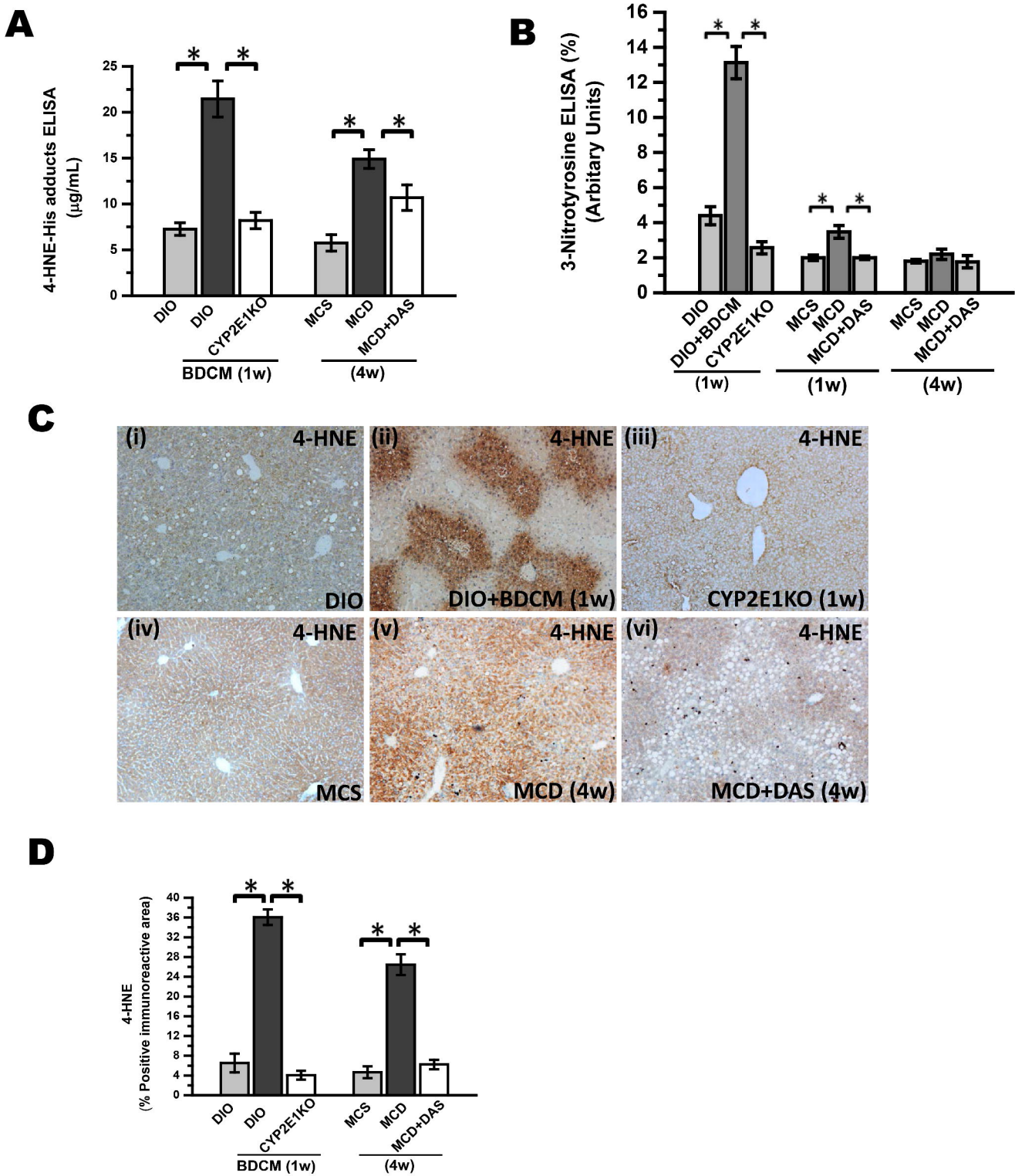
A
4-HNE-His adducts ELISA (μg/mL)
DIO
DIO
CYP2E1KO
MCS
MCD
MCD+DAS
BDCM (1w)
(4w)
B
3-Nitrotyrosine ELISA (%) (Arbitary Units)
DIO
DIO+BDCM
CYP2E1KO
MCS
MCD
MCD+DAS
(1w)
(1w)
(4w)
C
(i) 4-HNE DIO
(ii) 4-HNE DIO+BDCM (1w)
(iii) 4-HNE CYP2E1KO (1w)
(iv) 4-HNE MCS
(v) 4-HNE MCD (4w)
(vi) 4-HNE MCD+DAS (4w)
D
4-HNE (% Positive immunoreactive area)
DIO
DIO
CYP2E1KO
MCS
MCD
MCD+DAS
BDCM (1w)
(4w)

Fig. 2.

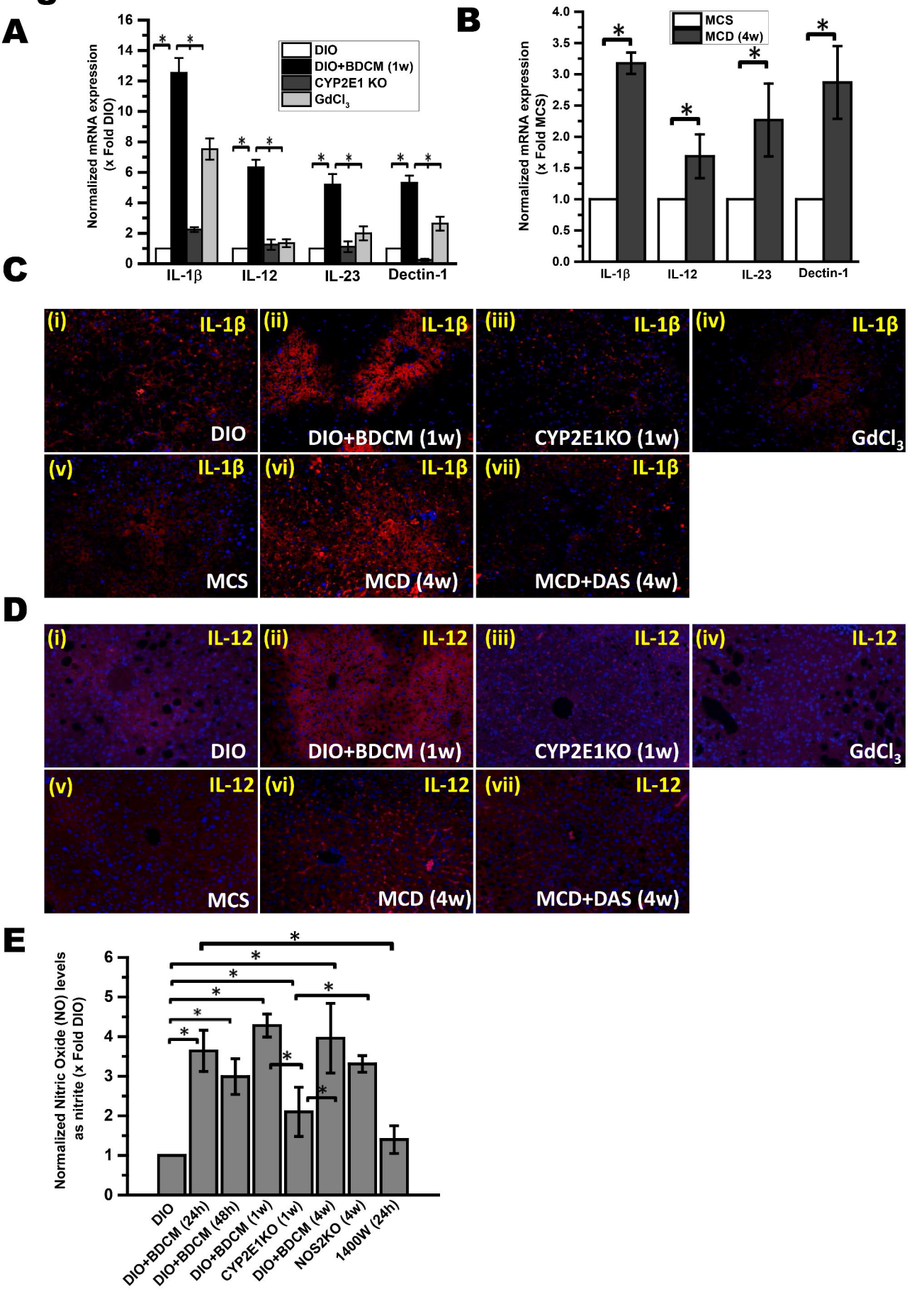
A
Normalized mRNA expression (x Fold DIO)
DIO
DIO+BDCM (1w)
CYP2E1 KO
GdCl3
IL-1β
IL-12
IL-23
Dectin-1
B
Normalized mRNA expression (x Fold MCS)
MCS
MCD (4w)
IL-1β
IL-12
IL-23
Dectin-1
C
(i) IL-1β DIO
(ii) IL-1β DIO+BDCM (1w)
(iii) IL-1β CYP2E1KO (1w)
(iv) IL-1β GdCl3
(v) IL-1β MCS
(vi) IL-1β MCD (4w)
(vii) IL-1β MCD+DAS (4w)
D
(i) IL-12 DIO
(ii) IL-12 DIO+BDCM (1w)
(iii) IL-12 CYP2E1KO (1w)
(iv) IL-12 GdCl3
(v) IL-12 MCS
(vi) IL-12 MCD (4w)
(vii) IL-12 MCD+DAS (4w)
E
Normalized Nitric Oxide (NO) levels as nitrite (x Fold DIO)
DIO
DIO+BDCM (24h)
DIO+BDCM (48h)
DIO+BDCM (1w)
CYP2E1KO (1w)
DIO+BDCM (4w)
NOS2KO (4w)
1400W (24h)

Fig. 3.

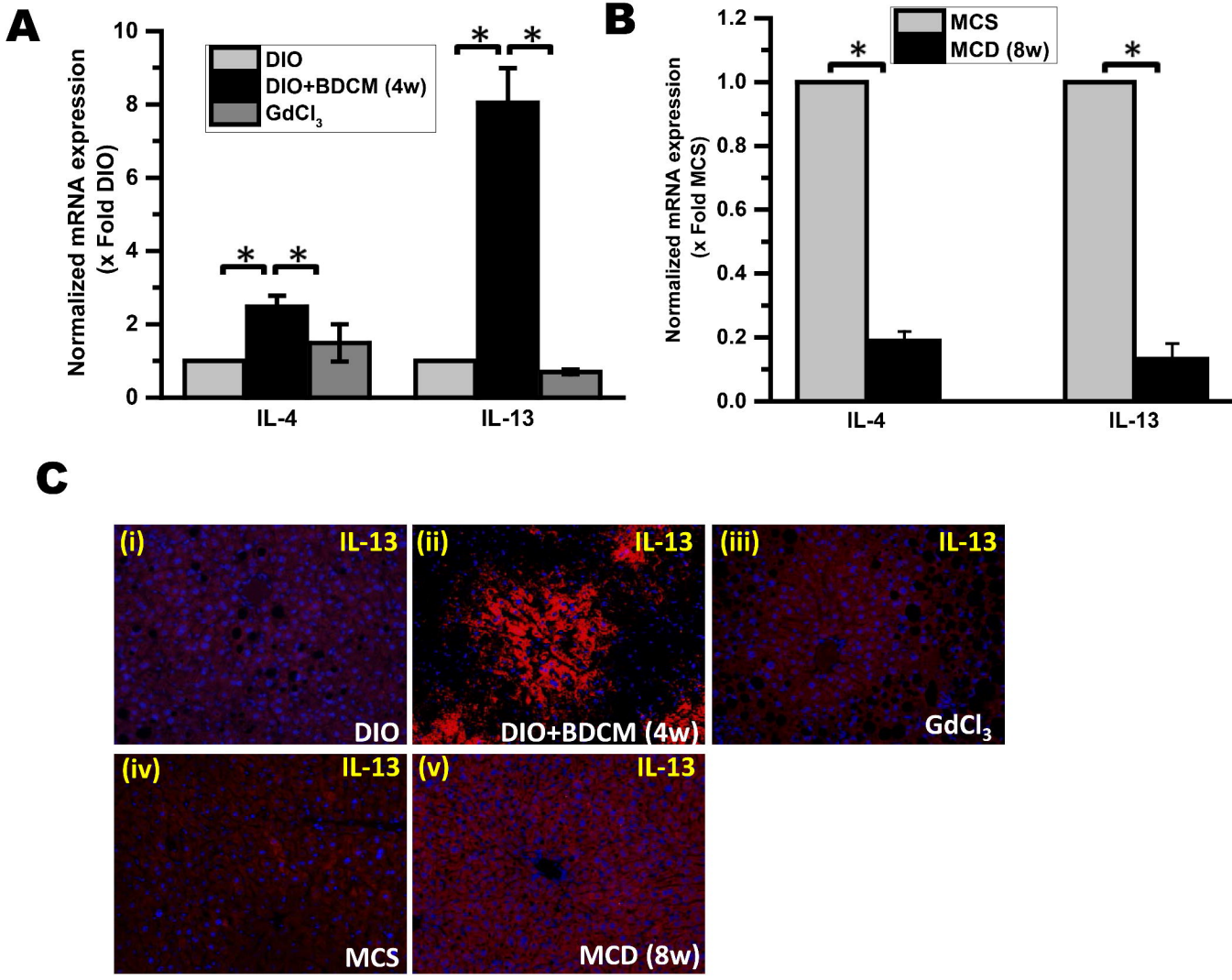
A
Normalized mRNA expression
(x Fold DIO)
DIO
DIO+BDCM (4w)
GdCl3
IL-4
IL-13
B
Normalized mRNA expression
(x Fold MCS)
MCS
MCD (8w)
IL-4
IL-13
C
(i) IL-13 DIO
(ii) IL-13 DIO+BDCM (4w)
(iii) IL-13 GdCl3
(iv) IL-13 MCS
(v) IL-13 MCD (8w)

Fig. 4.

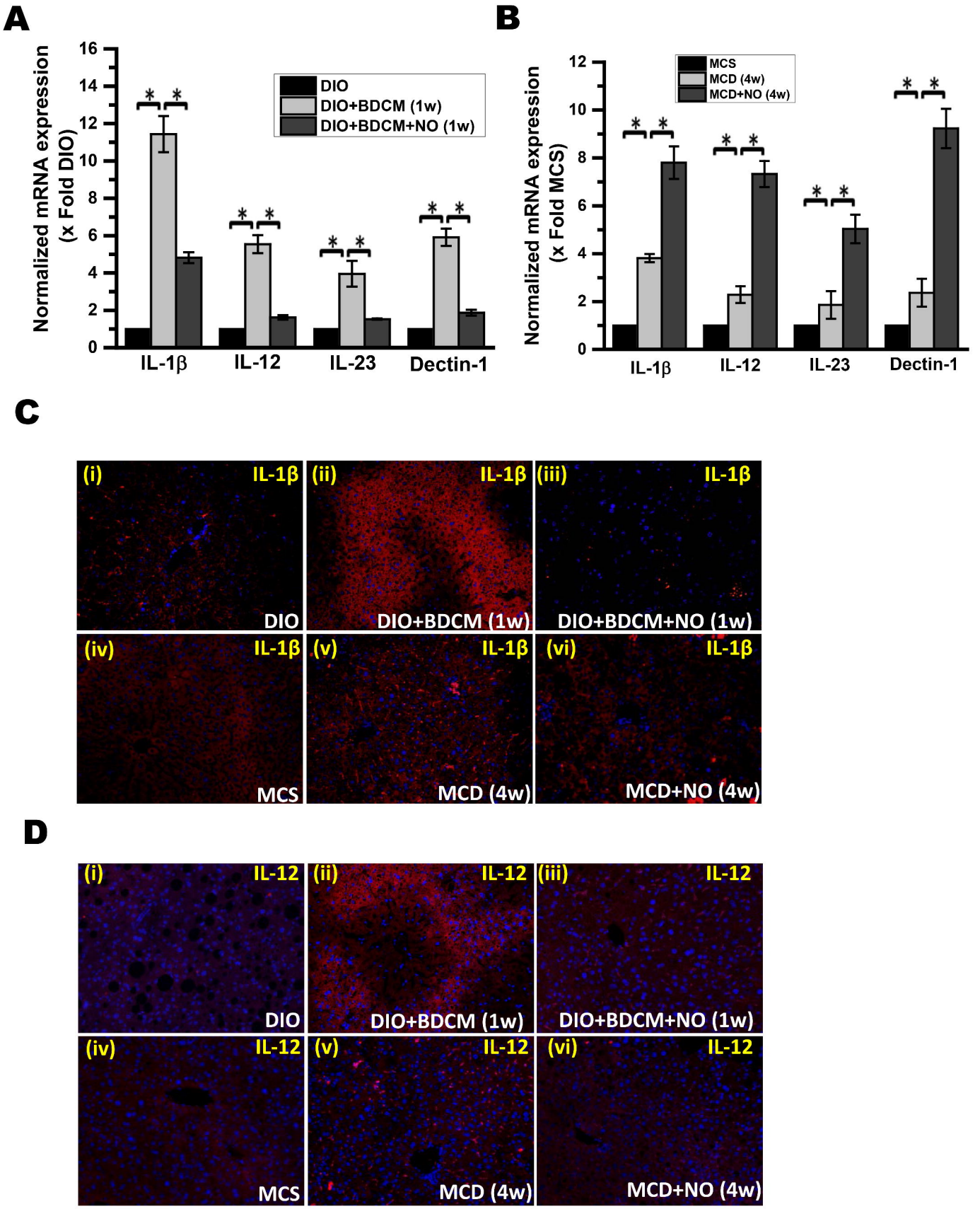
A
Normalized mRNA expression (x Fold DIO)
DIO
DIO+BDCM (1w)
DIO+BDCM+NO (1w)
IL-1β
IL-12
IL-23
Dectin-1
B
Normalized mRNA expression (x Fold MCS)
MCS
MCD (4w)
MCD+NO (4w)
IL-1β
IL-12
IL-23
Dectin-1
C
(i) IL-1β DIO
(ii) IL-1β DIO+BDCM (1w)
(iii) IL-1β DIO+BDCM+NO (1w)
(iv) IL-1β MCS
(v) IL-1β MCD (4w)
(vi) IL-1β MCD+NO (4w)
D
(i) IL-12 DIO
(ii) IL-12 DIO+BDCM (1w)
(iii) IL-12 DIO+BDCM+NO (1w)
(iv) IL-12 MCS
(v) IL-12 MCD (4w)
(vi) IL-12 MCD+NO (4w)

Fig. 5.

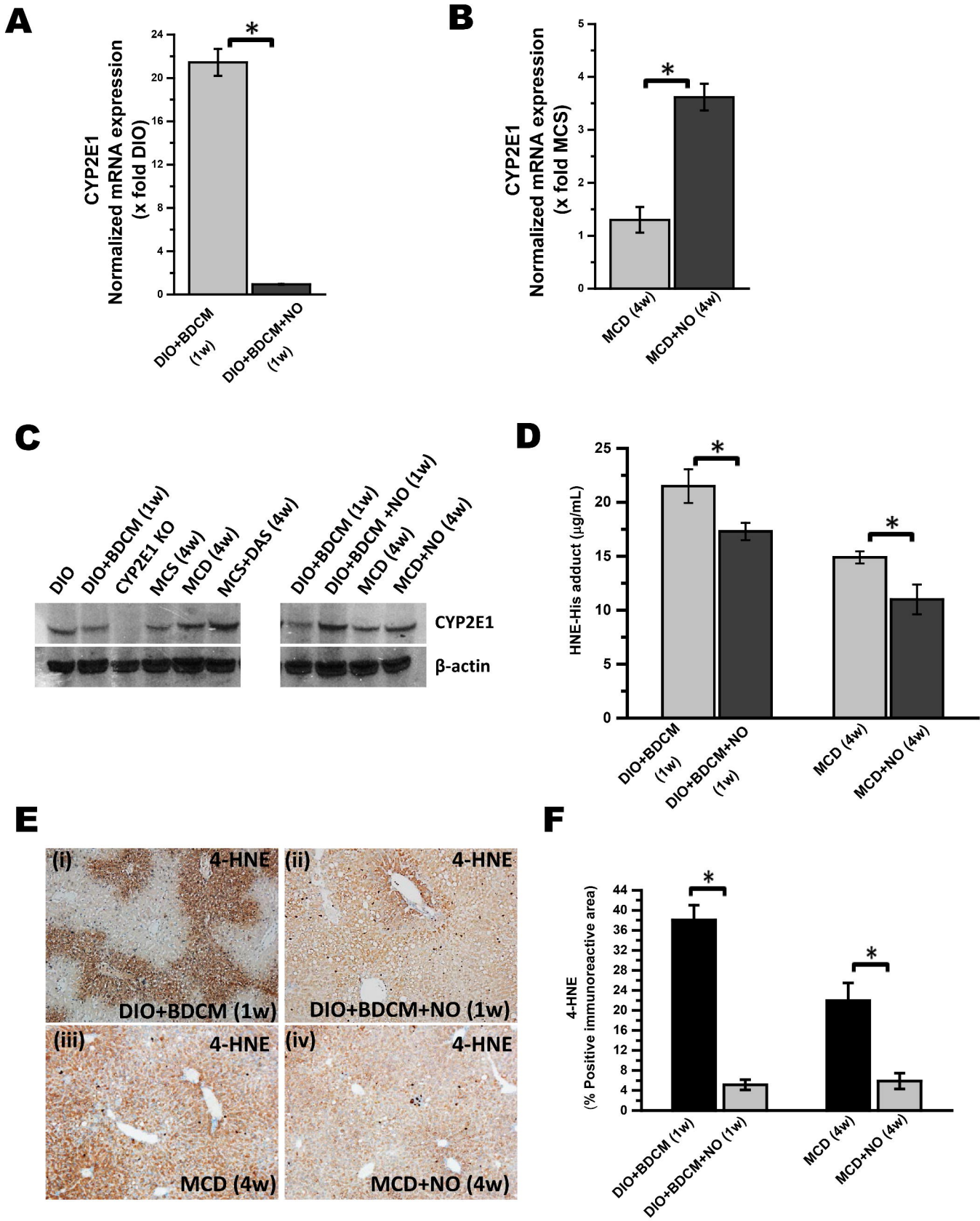
A
CYP2E1
Normalized mRNA expression
(x fold DIO)
24
20
16
12
8
4
0
*
DIO+BDCM
(1w)
DIO+BDCM+NO
(1w)
B
CYP2E1
Normalized mRNA expression
(x fold MCS)
5
4
3
2
1
0
*
MCD (4w)
MCD+NO (4w)
C
DIO
DIO+BDCM (1w)
CYP2E1 KO
MCS (4w)
MCD (4w)
MCS+DAS (4w)
DIO+BDCM (1w)
DIO+BDCM +NO (1w)
MCD (4w)
MCD+NO (4w)
CYP2E1
β-actin
D
HNE-His adduct (μg/mL)
25
20
15
10
5
0
*
*
DIO+BDCM
(1w)
DIO+BDCM+NO
(1w)
MCD (4w)
MCD+NO (4w)
E
(i)
4-HNE
DIO+BDCM (1w)
(ii)
4-HNE
DIO+BDCM+NO (1w)
(iii)
4-HNE
MCD (4w)
(iv)
4-HNE
MCD+NO (4w)
F
4-HNE
(% Positive immunoreactive area)
44
40
36
32
28
24
20
16
12
8
4
0
*
*
DIO+BDCM (1w)
DIO+BDCM+NO (1w)
MCD (4w)
MCD+NO (4w)

Fig. 6.

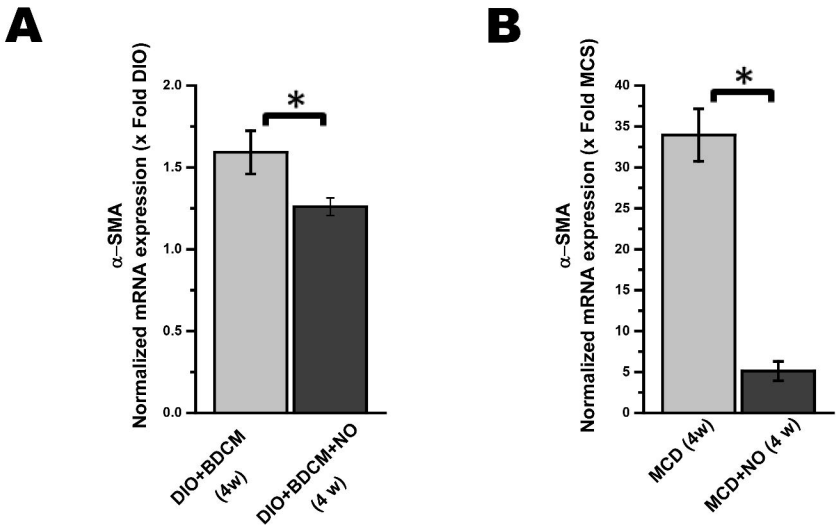

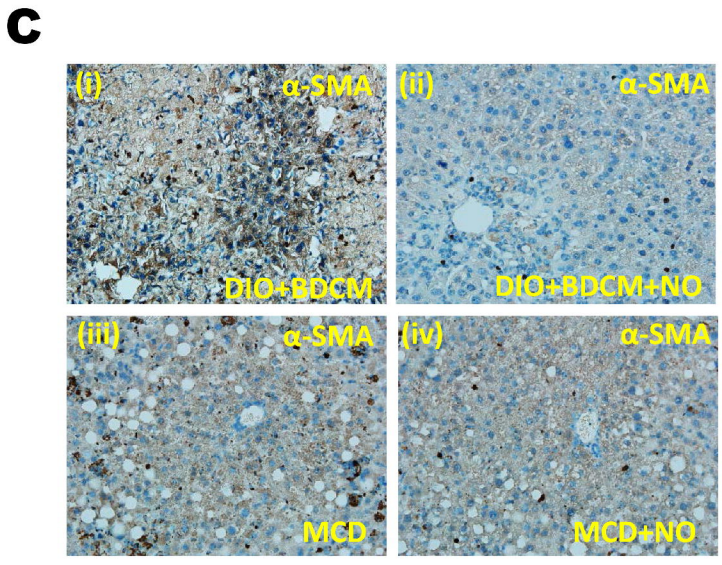

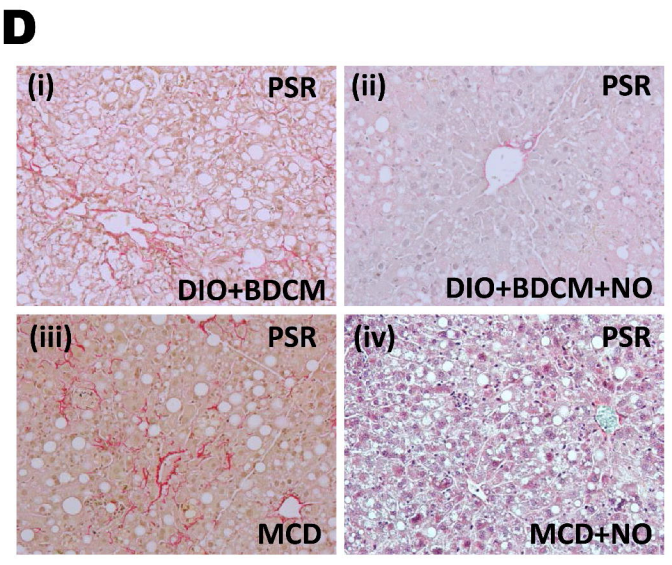

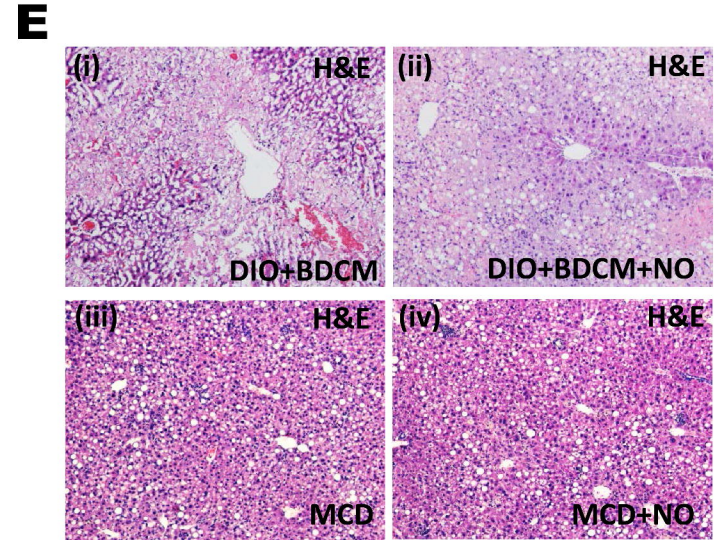

F

NASH CRN score for NASH model						
	DIO	DIO +BDCM	DIO +BDCM +NO	MCS	MCD	MCD +NO
Steatosis	2	3	1	1	3	2
Lobular Inflammation	1	3	0	0	2	1
Hepatocyte Ballooning	1	2	1	1	2	1
Stage of Fibrosis	1C	3	1A	1A	2	1C

1A:Mild; 1C: Portal, Periportal Fibrosis, 3: Bridging Fibrosis

Fig. 7.

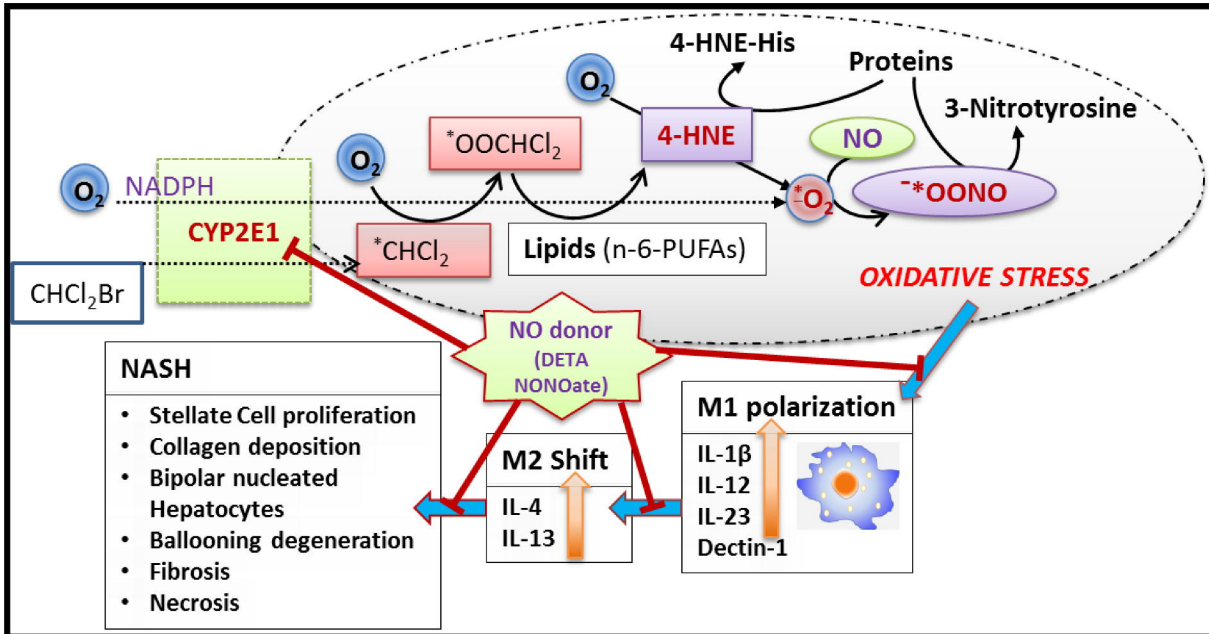
4-HNE-His
Proteins
3-Nitrotyrosine
O_2
4-HNE
NO
$^{*}OOCHCl_2$
O_2
$^{*}O_2^{-}$
$^{-}{}^{*}OONO$
O_2
NADPH
CYP2E1
$^{*}CHCl_2$
Lipids (n-6-PUFAs)
$CHCl_2Br$
OXIDATIVE STRESS
NO donor
(DETA
NONOate)
NASH
• Stellate Cell proliferation
• Collagen deposition
• Bipolar nucleated Hepatocytes
• Ballooning degeneration
• Fibrosis
• Necrosis
M2 Shift
IL-4
IL-13
M1 polarization
IL-1β
IL-12
IL-23
Dectin-1